2024 IEEE/RSJ International Conference on Intelligent Robots and Systems (IROS)
October 14-18, 2024. Abu Dhabi, UAE

A Tactile Lightweight Exoskeleton for Teleoperation: Design and Control Performance

Moein Forouhar, Hamid Sadeghian, Daniel Perez Suay, Abdeldjallil Naceri, and Sami Haddadin

***Abstract*— In this work, an upgraded exoskeleton design is presented with enhanced trajectory tracking and mechanical transparency. Compared to the first version, the design features a 3-DoF actuated shoulder joint and a mechanism to regulate the pretension of Bowden cables. Force/torque sensors are installed to directly measure the interaction forces between the human arm and the exoskeleton at the connecting points. Three control strategies were evaluated to follow a desired trajectory; A PD controller, a PD controller with friction observer, and an adaptive controller based on Radial Basis Function (RBF). These strategies also form the basis for an admittance control, aimed at improving the exoskeleton's mechanical transparency during interaction with the human arm. Simulations and experimental results demonstrate that the PD control, supported by friction estimation via a momentum observer, achieves superior tracking performance. Moreover, the system's mechanical transparency is enhanced using the admittance RBF-based controller, showing marginally superior results.**

I. Introduction

Service robots are advancing in hardware and communication, leading to increased use in telemedicine. Several factors contribute to the success of telemedicine, with haptic feedback being a crucial component. Haptic interfaces enable doctors and other operators to send position commands to the service robot and receive force feedback (Fig. 1). This is essential for examinations that require a doctor's sense of touch, such as tele-diagnostics. Although haptic interfaces help operators perform their tasks precisely, most of them have a limited range of motion, which might not be suitable for some examinations, especially those involving upper and lower limb examinations (e.g., shoulder or knee). However, haptic exoskeletons can cover the full range of movement of the human arm, as illustrated in Fig. 2. These exoskeletons can map the human arm pose to the remote robot arm by using joint angles and similarly map the interaction forces from the remote robot system to the human arm [2].

All authors are with the Munich Institute of Robotics and Machine Intelligence, Technical University of Munich, 80992 Munich, Germany. H. Sadeghian is also with the Faculty of Engineering, University of Isfahan, 8174673441 Isfahan. Corresponding Author: hamid.sadeghian@tum.de

We gratefully acknowledge the funding of the Lighthouse Initiative Geriatronics by StMWi Bayern (Project X, grant no. IUK-1807-0007//IUK582/001) and LongLeif GaPa gGmbH (Project Y). The authors acknowledge the financial support by the Federal Ministry of Education and Research of Germany (BMBF) in the program of "Souverän. Digital. Vernetzt." Joint project 6G-life, project identification number 16KISK002. The paper also funded by the German Research Foundation (DFG, Deutsche Forschungsgemeinschaft) as part of Germany's Excellence Strategy – EXC 2050/1 – Project ID 390696704 – Cluster of Excellence "Centre for Tactile Internet with Human-in-the-Loop" (CeTI) of Technische Universität Dresden.

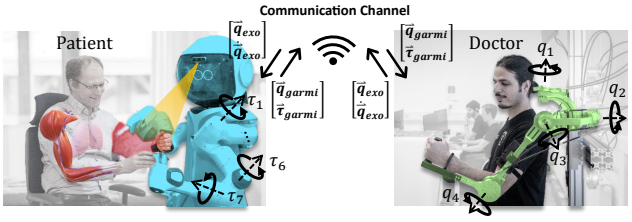

Fig. 1: The proposed 4-DOF exoskeleton, worn by an operator to control the remote service robot GARMI [1], in a bilateral teleoperation.

This mapping can cover the entire human arm workspace, allowing the replication of complex gestures that desktop haptic devices may struggle to support due to workspace limitations or restricted degrees of freedom. Consequently, these exoskeletons are not confined to specific gestures but can accommodate a wide range of telemedicine applications.

Many exoskeleton designs use direct actuation at the joints. However, these designs often result in bulky and heavy systems because they must support both motor weights and the exoskeleton payload. In contrast, tendon-driven wearable robots offer a promising alternative. For example, in soft exosuits [3], tendons are routed through textile channels to the target joint to generate translational forces, with the human skeleton providing structural support. For more accurate motions, tendons can be guided through channels supported by pulleys and linkages to minimize friction and maximize the rigidity of the guiding paths [4]. However, an efficient approach that combines the simplicity of soft exosuits with the accuracy of tendon-driven exoskeletons is using Bowden cables as a transmission mechanism. This method provides a lightweight structure with high actuation power [5].

Various steps should be taken to increase the mechanical transparency of tendon-driven upper limb exoskeletons. One step involves friction compensation. A general framework for friction identification in industrial manipulators is proposed by [6]. For tendon-driven systems, [7] presented a friction loss model based on the overall curvature in Bowden cables. A more complex model proposed by the authors of the current work [8] considers both the cable pretension and curvature on the friction and torque efficiency. Another model-based friction compensation uses disturbance estimation methods to estimate the friction. In [9], a disturbance observer without restrictions on degrees of freedom or requiring an exact dynamic model is designed which can estimate ex-

ternal disturbances, including friction in the joints. Similarly, the momentum observer method, as described by [10], is a powerful method that detects and isolates actuator faults and provides efficient collision detection using proprioceptive sensors.

Improving the system's sensors also plays a role in enhancing mechanical transparency. In [11], the authors embedded an auxiliary wire in the Bowden-cable, called a sensing wire, to measure displacement changes and thus, estimate the overall Bowden-cable curvature. Another work [12] implements joint torque sensors in a custom-made cable-driven exoskeleton to improve the user intention estimation. To optimally use force/torque sensors, the authors in [13] present a sensor reduction technique utilizing a Kalman filter-based sensor fusion system for admittance control.

Compliance in the joints and transmission dynamics is another critical area. In [14], a method is proposed to allow articulated soft robots with nonlinear spring characteristics to be treated as "quasi-fully" actuated. Alternatively, in [15], the authors combined the Singular Perturbation method and Model Predictive Control (MPC) to control flexible-joint robots. The paper [16] presented a motor-driven tendon-sheath artificial muscle with a compliant structure and variable elasticity, inspired by the Hill muscle model.

Nonlinear control approaches are essential for compensating unmodeled dynamics. A hierarchical control strategy for cable-driven upper limb exosuits, proposed by [17], includes layers for active impedance control, backlash compensation, and actuation driving. A robust adaptive controller for accurate trajectory tracking with inertia and load uncertainties is developed [18]. Similarly, [19] introduced a novel sliding mode controller using nonlinear model-based switching functions for improved torque inputs and robustness. Finally, the work [20] employs admittance controllers to integrate human operator and environmental interactions in the control loop.

This study introduces the second version of a lightweight tactile upper limb exoskeleton that uses Bowden cables for remote actuation. Compared to its first version [21], this version includes several mechatronic improvements, such as an additional actuated degree of freedom on the shoulder joint, a mechanism for adjusting the pretension of the Bowden cables, and force/torque sensors at the connection between the arm and the exoskeleton. The dynamics of the exoskeleton are derived and simulated using MATLAB Simulink. The momentum observer method is implemented to estimate friction in the remote actuation system for friction estimation in the Bowden cables, and an adaptive RBF (Radial Basis Function) method is used to reject unmodeled dynamics. Three controllers for trajectory following and admittance control are developed and verified through simulation. Finally, the findings are validated through real-world experiments.

II. Modeling and Control

The exoskeleton is described by a serial kinematic chain of rigid links with joint coordinates denoted by $\boldsymbol{q} \in \mathbb{R}^{4\times 1}$ (Fig. 2). To obtain the transformation matrices, frames were

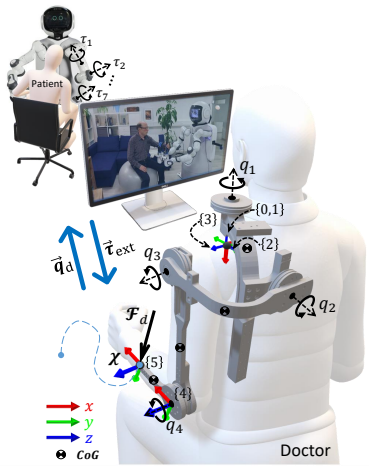

Fig. 2: The kinematic structure of the exoskeleton including 3 Dof gimbal joints in the shoulder and 1 Dof elbow joint. The joint angles and coordinate frames are illustrated. Having this structure, a remote robot is used as an avatar of the user with haptic feedback.

TABLE I: D-H parameters of the exoskeleton

Link Number	$\alpha_{i-1}[rad]$	$a_{i-1}[m]$	$d_i[m]$	$\theta_i[rad]$
1	0	0	0	q_1
2	$\frac{\pi}{2}$	0	0	$q_2 - \frac{\pi}{2}$
3	$\frac{\pi}{2}$	0	0	q_3
4	0	0.360	0.149	$q_4 - \frac{\pi}{2}$

assigned to each joint, and Table I was completed using the modified D-H convention [22]. The dynamic equation of the exoskeleton is given by,

$$\boldsymbol{M}(\boldsymbol{q})\ddot{\boldsymbol{q}} + \boldsymbol{C}(\boldsymbol{q},\dot{\boldsymbol{q}})\dot{\boldsymbol{q}} + \boldsymbol{g}(\boldsymbol{q}) + \boldsymbol{\tau}_{\text{friction}} + \boldsymbol{\tau}_{\text{ext}} = \boldsymbol{\tau}_{\text{motor}}, \quad (1)$$

where $\boldsymbol{M}(\boldsymbol{q})$ denotes the inertia matrix, $\boldsymbol{C}(\boldsymbol{q},\dot{\boldsymbol{q}})$ denotes the Coriolis/centrifugal matrix, $\boldsymbol{g}(\boldsymbol{q})$ denotes the gravity vector, $\boldsymbol{\tau}_{\text{friction}}$ denotes the torque on the motor due to friction, $\boldsymbol{\tau}_{\text{ext}}$ denotes the external torques on the exoskeleton, and $\boldsymbol{\tau}_{\text{motor}}$ denotes the torque produced by the actuators.

Each link in the exoskeleton has 10 calibration parameters, including mass, center of gravity (CoG) position, and moment of inertia. Identifying these parameters can be challenging, especially in the presence of friction. However, for simplicity, the parameters were taken directly from the exoskeleton's CAD data. The values can be found in Table II and Table III. The dynamic model of (1) is then obtained, as outlined in [23].

TABLE II: Mass and Position Vectors for each index i

i	m_i[kg]	${}^i\vec{\boldsymbol{r}}_{\boldsymbol{G_i}}$[m]
1	0.692	$[-0.022, -0.118, 0.025]^T$
2	0.729	$[0.0, -0.065, 0.119]^T$
3	0.782	$[0.195, 0.0, 0.108]^T$
4	0.464	$[0.014, 0.0, -0.017]^T$

TABLE III: The moment of inertia values for the links $\boldsymbol{I}_i[10^{-3}kg.m^2]$

$\boldsymbol{I}_1$			$\boldsymbol{I}_2$		
29	−0.1	−0.2	7.3	0.0	0.0
−0.1	1.6	1.2	0.0	4.2	2.8
−0.2	1.2	2.2	0.0	2.8	3.5
$\boldsymbol{I}_3$			$\boldsymbol{I}_4$		
0.3	0.0	−1.0	0.2	0.0	0.0
0.0	19.6	0.0	0.0	0.8	0.0
−1.0	0.0	19.7	0.0	0.0	1.0

The next step is to identify the external force $\boldsymbol{\tau}_{\text{ext}}$ and friction $\boldsymbol{\tau}_{\text{friction}}$ in the dynamic model. An effective method for identifying these disturbances is the momentum observer. The observer calculates the residual value $\boldsymbol{r}(t)$, which exponentially converges to $(\boldsymbol{\tau}_{\text{friction}} + \boldsymbol{\tau}_{\text{ext}})$ as,

$$\boldsymbol{r}(t) = \boldsymbol{K}_I \left[\boldsymbol{p}(t) - \int_0^t \left(\boldsymbol{\tau} + \boldsymbol{C}^T(\boldsymbol{q}, \dot{\boldsymbol{q}})\dot{\boldsymbol{q}} - \boldsymbol{g}(\boldsymbol{q}) + \boldsymbol{r}(\sigma) \right) d\sigma \right] \tag{2}$$

$$\dot{\boldsymbol{r}} = -\boldsymbol{K}_I \boldsymbol{r} - \boldsymbol{K}_I(\boldsymbol{\tau}_{\text{ext}+}\boldsymbol{\tau}_{\text{f}}) \tag{3}$$

where $\boldsymbol{p}(t) = \boldsymbol{M}\dot{\boldsymbol{q}}$ is the generalized momentum of the system and $\boldsymbol{K}_I$ is a diagonal positive matrix [24]. To subtract the external torque from the residual value in (2), a dedicated F/T sensor is required to directly measure the external wrench and then determine the friction in the joints.

A. Control of Exoskeleton

Two control scenarios have been devised for the exoskeleton. In the first one, the exoskeleton is commanded to follow a predefined trajectory in the task space. The controller should be robust with respect to the unmodeled dynamics and achieve good performance in the trajectory-following. In the second scenario, the exoskeleton remains stationary, only displaying compliance in response to external forces exerted by the user's arm. The primary objective of this controller is to minimize the interaction forces between the user and the exoskeleton.

1) PD Controller with Gravity Compensation: The primary control scheme utilizes a low-gain PD controller and a gravity compensation term to counteract gravitational forces. The error between the desired joint trajectories and the current joint positions and velocities generates a control effort for the actuators. The control gains are listed in Table IV. The gravity compensation term is obtained from the dynamics model.

2) PD Controller with Friction Compensation: The second control scheme uses friction estimation, obtained from a momentum observer, as a feedforward term to the PD controller designed in the previous step. As the friction is relatively high in this system due to the use of Bowden cable, compensating for this disturbance significantly reduces the tracking error. The value of the momentum observer gain is given in Table IV. To map the external forces to external torques, the Jacobian at the sensor positions should be used. The external torques from both force/torque sensors, given by

$$\boldsymbol{\tau}_{\text{ext}} = \boldsymbol{J}_{\text{elbow}}^T \boldsymbol{f}_{\text{elbow}} + \boldsymbol{J}_{\text{hand}}^T \boldsymbol{f}_{\text{hand}} \tag{4}$$

is then be subtracted from the residual value of the momentum observer to obtain the overall friction in the joints.

3) Trajectory Following with Radial Basis Functions (RBF): The third controller employed for trajectory following utilizes RBF. Following the approach discussed in [25], the combined error $\boldsymbol{s} = \dot{\tilde{\boldsymbol{q}}} + \lambda\tilde{\boldsymbol{q}}$ is defined, where $\tilde{\boldsymbol{q}}$ represents the tracking error. The weights of the RBFs are adjusted as,

$$\begin{aligned} \varphi_j(\boldsymbol{x}) &= \exp\left(-\frac{\|\boldsymbol{x} - \boldsymbol{m}_j\|^2}{2b_j^2} \right), \\ \boldsymbol{\tau}_{RBF} &= \boldsymbol{W}\boldsymbol{\varphi}^T, \\ \dot{\boldsymbol{W}} &= \beta \boldsymbol{s}\boldsymbol{\varphi}, \end{aligned} \tag{5}$$

where $\boldsymbol{W}$ is the RBF weighting matrix of size $4 \times N$, with N as the number of functions and $\boldsymbol{\varphi}(\boldsymbol{x}) = [\varphi_1(\boldsymbol{x}), \varphi_2(\boldsymbol{x}), \ldots, \varphi_N(\boldsymbol{x})]$. The $\boldsymbol{m}_j$ denote the RBF centers, which are randomly selected within the state domain $\boldsymbol{x} = [\boldsymbol{q}, \dot{\boldsymbol{q}}]^T$. Although b_j may vary for each center, a uniform value is used in this problem. The initial value of $\boldsymbol{W}$ is set as a random matrix. The parameters used in this controller are summarized in Table IV.

TABLE IV: Control Parameters

Parameter	Value
K_p	50
K_d	20
K_I	15.0
$\boldsymbol{m}_j$ (Experiment)	8×50 random values
$\boldsymbol{m}_j$ (Simulation)	8×100 random centers
b_j	1.2
λ	20
Learning Rate	20

4) Admittance Control: For mechanical transparency, the following admittance model is employed to achieve compliant behavior for the interaction forces between the human arm and the exoskeleton,

$$\boldsymbol{M}_d\ddot{\tilde{\boldsymbol{q}}} + \boldsymbol{D}_d\dot{\tilde{\boldsymbol{q}}} + \boldsymbol{K}_d\tilde{\boldsymbol{q}} = \boldsymbol{\tau}_{\text{ext}}. \tag{6}$$

Here, $\boldsymbol{M}_d$, $\boldsymbol{D}_d$, and $\boldsymbol{K}_d$ represent the desired inertia, damping, and stiffness matrices, respectively. The term $\tilde{\boldsymbol{q}} = \boldsymbol{q}_{ref} - \boldsymbol{q}$ is the joint space error in generating a reference trajectory, and $\boldsymbol{\tau}_{\text{ext}}$ denotes the external torque applied to the exoskeleton due to the interaction between the exoskeleton and the arm.

A lower admittance will cause lower resistance to interaction forces and, as a result, higher mechanical transparency for haptic feedback. High admittance values may cause instability, so the passivity of the system should be preserved [20]. The reference trajectory derived from this admittance model is utilized as a reference input for the trajectory-following controllers designed in earlier sections, thereby realizing the mass-spring-damper model (6) between the arm and the exoskeleton.

III. Simulation Study

A. Arm-Exoskeleton Simulation

The connection between the arm and the exoskeleton is modeled as a spring damper. The human arm is modeled as a serial kinematic chain with a three DoF gimbal joint at the shoulder and a singular revolute joint at the elbow, as illustrated in Fig. 3. It is assumed that the interaction forces do not affect human arm motion. Additionally, the center of the shoulder is assumed to have 5 cm offset from the exoskeleton's corresponding shoulder point. The free length of the spring model matches this offset distance. The parameters of the exoskeleton are derived from its CAD model, and nominal values are selected for the stiffness and damping of the exoskeleton-arm connection models. To simplify modeling, both centrifugal and Coriolis terms in the dynamic model are assumed to be negligible, and the focus is primarily on the inertial and gravitational forces and the friction in the joints. Moreover, a general model for the friction in the joints [26] was exploited.

MATLAB Simulink was used for the simulations. The `ode1` (Euler) solver with a fixed step size of 0.001 seconds was selected, reflecting the step size of a real-time controller. For the trajectory following, the simulation input is the desired joint trajectories, whereas for the simulation of mechanical transparency, the input is the desired task-space trajectory of the human arm. Due to the spring-damper connection model, the exoskeleton follows the arm's motion according to its dynamics. The controllers are detailed in the following sections.

B. Trajectory following

Three controllers were examined to enhance the trajectory-following performance of the exoskeleton. The first controller implements a low-gain PD control with a gravity compensation to track a desired joint trajectory derived from the inverse kinematics of a circular path in the task space. However, the presence of friction leads to a significant tracking error, causing the end-effector to deviate from the designated circular path. To address this, the second controller augments the low-gain PD controller with a friction compensator based on momentum observer friction estimation. This approach significantly reduces the tracking error. The third controller uses an adaptive control strategy based on an RBF described in (5). The controller updates its weighting matrices based on the mentioned intermediate variable to reduce the task-space tracking error. As depicted in Fig. 4, simulation results demonstrate that the low-gain PD controller alone is unable to track the desired trajectory, whereas both the low-gain PD controller with friction compensation and the RBF-based strategy achieve good tracking performance.

C. Mechanical transparency improvement

An admittance controller can help minimize the interaction forces between the human arm and the exoskeleton. All three trajectory-following controllers can be utilized for the admittance controller. However, the transparency simulation specifically focuses on the RBF controller for designing

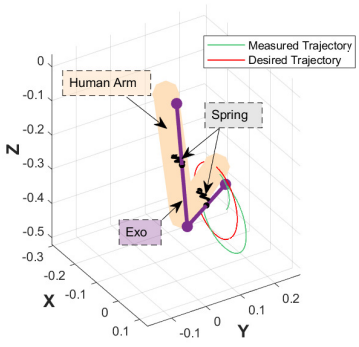

Fig. 3: The model of the exoskeleton and human arm in simulation. The connection between the exoskeleton and the human arm is modeled as a spring-damper system with $K = 2000$ N.m and $D = 20$ N.s/m.

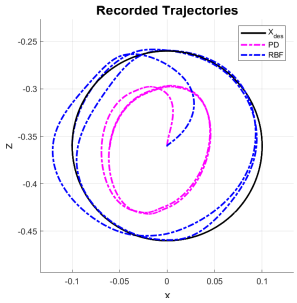

Fig. 4: Simulation comparing the tracking performance of the exoskeleton under two control strategies. Initially, the RBF controller exhibits poor performance due to the need for its weighting matrices to converge. However, once the weighting matrices are properly adapted to the tracking error, it outperforms the PD controller in tracking performance.

the centers of its weighting matrix, while the other two controllers are evaluated through real-world experiments. As shown in Fig. 4, the RBF+PD controller demonstrates effective trajectory following. Based on the admittance model in (6), the desired trajectory is computed to achieve compliant behavior in response to the external torque, τ_{ext}. The results are illustrated in Fig. 5. The interaction forces between the arm and the exoskeleton are mapped to joint space to provide a better understanding of the transparency performance. The controller is activated for the first 10 seconds to reduce the interaction torque between the arm and the exoskeleton. At $t = 10s$, the controller is deactivated to demonstrate its effect on interaction torques in the absence of the admittance controller. The plots show that the admittance controller with RBF reduces the interaction forces between the exoskeleton and the human arm.

IV. Experimental Study

A. Exoskeleton Setup

Similar to the first exoskeleton version [21], Bowden cables were utilized for the remote actuation of the links. As

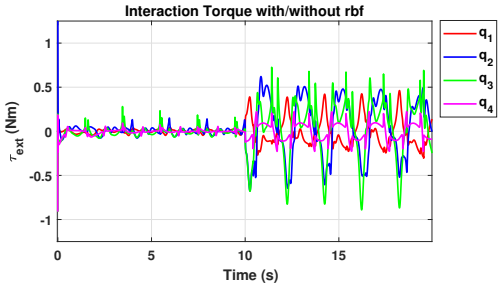

Fig. 5: Interaction force between the exoskeleton and the arm. For the initial 10 seconds, the exoskeleton actuators track a desired trajectory, which is updated based on the interaction torque using RBF and PD disturbance rejection methods. At $t = 10s$, the exoskeleton actuators become inactive, leading to a substantial increase in the interaction force across all four joints.

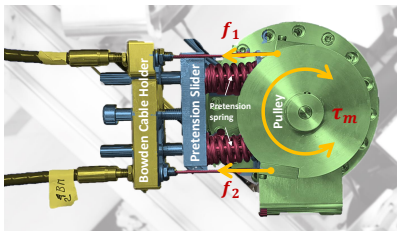

Fig. 6: The pretension mechanism adjusts the tension in both Bowden cables to remove any slack when the direction of motion changes. The pretension is adjusted using a screw that presses two springs with a stiffness of $K = 39.46$ N/mm.

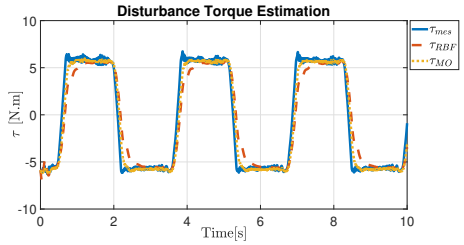

Fig. 7: Torque estimation comparison. Since the inertial and gravitational terms are much smaller than the friction in the system, the estimated friction closely aligns with the motor torque values τ_{mes}. Notably, the momentum observer achieves faster convergence compared to the RBF method.

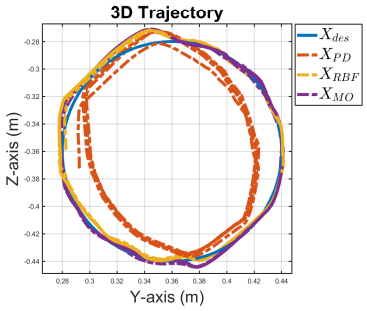

Fig. 8: The low-gain PD controller with friction compensation (using the momentum observer) demonstrates the best performance, closely followed by the adaptive RBF controller. In contrast, the low-gain PD controller alone exhibits the lowest performance.

a result, thinner links were designed since the links do not need to support the weight of the actuators. However, the use of Bowden cables introduces friction between the actuators and the joints, and the thin design of the links results in structural flexibility. As discussed earlier, the friction is compensated with a feedforward term in the controller using a momentum observer. Moreover, since the exoskeleton is attached to the human arm, the flexibility of the links is damped. The motors can produce a maximum torque of 87 N·m and a speed of 2.17 rad/s. However, to ensure safety, their limits are set to 20 N·m and 1 rad/s, respectively. The motors are equipped with both angle and torque sensors and have demonstrated good performance in tracking velocity and torque. For this experiment, the motors are configured in torque control mode.

Torque is transmitted to the link side via pulleys located on both the motor and the exoskeleton's joints. To improve transmission performance, a mechanism, as illustrated in Fig. 6, has been designed to regulate the pretension in the Bowden cables. This regulation is essential for ensuring the experiments' repeatability and friction modeling. Two F/T sensors were used to measure the interaction between the exoskeleton and the user's arm at a frequency of 1 kHz. The values were then mapped to the joint space using the Jacobian at the sensor positions and considering their installation orientation.

The exoskeleton is mounted on a height-adjustable stand, which can be adjusted according to the user's height and posture (standing or sitting). This arrangement allows users to comfortably stand next to the exoskeleton and operate it using its handler. Velcro straps are utilized to securely fasten the user's arm to the exoskeleton at the F/T sensor adapters.

V. RESULTS

Fig. 7 compares the torque estimation between the momentum observer and the Radial Basis Function (RBF). Due to the lightweight design of the links and the significant friction in the Bowden cables, the inertial and gravitational terms in the exoskeleton dynamics can be neglected. As a result, both the momentum observer and the RBF converge to the torques measured by the actuator sensors. The results indicate that friction estimation using the momentum observer converges more quickly than the RBF method, making it a more effective approach for agile maneuvers.

As shown in Fig. 8, the low-gain PD controller has low tracking performance. However, adding a feedforward term from the momentum observer to compensate for friction significantly improves the tracking performance. The RBF controller also shows good tracking, even though it is slightly less effective than the momentum observer.

To evaluate the mechanical transparency of the system, the exoskeleton is moved arbitrarily. As shown in Fig. 9, system

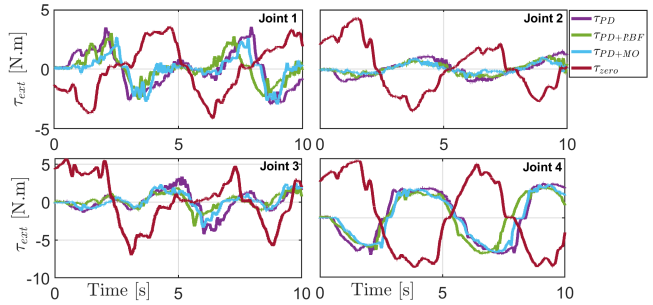

Fig. 9: Transparency results. Following an arbitrary trajectory, the interaction forces are mapped to exoskeleton joints. With zero motor torques, the highest interaction forces are felt. The admittance controllers (RBF, Momentum Observer, or PD), reduces the interaction forces by approximately 50%. Among the controllers, RBF outperforms in enhancing mechanical transparency.

transparency significantly decreases when zero torque is commanded to the actuators, primarily due to high joint friction. However, with the proposed admittance controllers, all three control approaches improve mechanical transparency, with the RBF controller demonstrating marginally superior performance.

VI. CONCLUSIONS

In this work, the mechatronic design of the exoskeleton and three different control strategies for task-space trajectory following were introduced. An admittance controller was also proposed to enhance mechanical transparency. The findings indicate that a low-gain PD controller performs poorly in tracking, while augmenting it with a friction compensation feed-forward term significantly improves tracking performance. Furthermore, when system modeling is imprecise, an adaptive RBF controller can achieve high tracking accuracy, even in the presence of significant friction within the Bowden cables. Moreover, the admittance controller enhances mechanical transparency across all three control strategies, with the RBF-based scheme exhibiting marginally superior transparency.

REFERENCES

[1] M. Tröbinger, C. Jähne, Z. Qu, J. Elsner, A. Reindl, S. Getz, T. Goll, B. Loinger, T. Loibl, C. Kugler *et al.*, "Introducing garmi-a service robotics platform to support the elderly at home: Design philosophy, system overview and first results," *IEEE Robotics and Automation Letters*, vol. 6, no. 3, pp. 5857–5864, 2021.

[2] J. Rebelo, T. Sednaoui, E. B. den Exter, T. Krueger, and A. Schiele, "Bilateral robot teleoperation: A wearable arm exoskeleton featuring an intuitive user interface," *IEEE Robotics Automation Magazine*, vol. 21, no. 4, pp. 62–69, 2014.

[3] K. Schmidt, J. E. Duarte, M. Grimmer, A. Sancho-Puchades, H. Wei, C. S. Easthope, and R. Riener, "The myosuit: Bi-articular anti-gravity exosuit that reduces hip extensor activity in sitting transfers," *Frontiers in neurorobotics*, vol. 11, p. 57, 2017.

[4] K. Shi, A. Song, and H. Li, "Optimized design for cable-driven shoulder-elbow exoskeleton robot," *IEEE Access*, vol. 9, pp. 68 197–68 207, 2021.

[5] V. Agrawal, W. J. Peine, and B. Yao, "Modeling of transmission characteristics across a cable-conduit system," *IEEE Transactions on Robotics*, vol. 26, no. 5, pp. 914–924, 2010.

[6] M. Indri and S. Trapani, "Framework for static and dynamic friction identification for industrial manipulators," *IEEE/ASME Transactions on Mechatronics*, vol. 25, no. 3, pp. 1589–1599, 2020.

[7] P. Letier, A. Schiele, M. Avraam, M. Horodinca, and A. Preumont, "Bowden cable actuator for torque-feedback in haptic applications," in *Proc. Eurohaptics*. Citeseer, 2006, pp. 1–6.

[8] D. Pérez-Suay, Y. Li, H. Sadeghian, A. Naceri, and S. Haddadin, "Torque transmission in double-tendon sheath driven actuators for application in exoskeletons," 2024.

[9] A. Mohammadi, M. Tavakoli, H. J. Marquez, and F. Hashemzadeh, "Nonlinear disturbance observer design for robotic manipulators," *Control Engineering Practice*, vol. 21, no. 3, pp. 253–267, 2013.

[10] A. De Luca, A. Albu-Schaffer, S. Haddadin, and G. Hirzinger, "Collision detection and safe reaction with the dlr-iii lightweight manipulator arm," in *2006 IEEE/RSJ International Conference on Intelligent Robots and Systems*. IEEE, 2006, pp. 1623–1630.

[11] U. Jeong and K.-J. Cho, "A novel low-cost, large curvature bend sensor based on a bowden-cable," *Sensors*, vol. 16, no. 7, p. 961, 2016.

[12] Y. Wang, A. Zahedi, Y. Zhao, and D. Zhang, "Extracting human-exoskeleton interaction torque for cable-driven upper-limb exoskeleton equipped with torque sensors," *IEEE/ASME Transactions on mechatronics*, vol. 27, no. 6, pp. 4269–4280, 2022.

[13] J. Sun, Y. Shen, and J. Rosen, "Sensor reduction, estimation, and control of an upper-limb exoskeleton," *IEEE Robotics and Automation Letters*, vol. 6, no. 2, pp. 1012–1019, 2021.

[14] M. Keppler, C. Ott, and A. Albu-Schäffer, "From underactuation to quasi-full actuation: Aiming at a unifying control framework for articulated soft robots," *International Journal of Robust and Nonlinear Control*, vol. 32, no. 9, pp. 5453–5484, 2022.

[15] M. Iskandar, C. van Ommeren, X. Wu, A. Albu-Schäffer, and A. Dietrich, "Model predictive control applied to different time-scale dynamics of flexible joint robots," *IEEE Robotics and Automation Letters*, vol. 8, no. 2, pp. 672–679, 2022.

[16] Q. Zhang, X. Wang, M. Tian, X. Shen, and Q. Wu, "Modeling of novel compound tendon-sheath artificial muscle inspired by hill muscle model," *IEEE Transactions on Industrial Electronics*, vol. 65, no. 8, pp. 6372–6381, 2017.

[17] B. K. Dinh, M. Xiloyannis, C. W. Antuvan, L. Cappello, and L. Masia, "Hierarchical cascade controller for assistance modulation in a soft wearable arm exoskeleton," *IEEE robotics and automation letters*, vol. 2, no. 3, pp. 1786–1793, 2017.

[18] J. Wang and O. R. Barry, "Inverse optimal robust adaptive controller for upper limb rehabilitation exoskeletons with inertia and load uncertainties," *IEEE Robotics and Automation Letters*, vol. 6, no. 2, pp. 2171–2178, 2021.

[19] C. Fallaha, M. Saad, J. Ghommam, and Y. Kali, "Sliding mode control with model-based switching functions applied on a 7-dof exoskeleton arm," *IEEE/ASME Transactions On Mechatronics*, vol. 26, no. 1, pp. 539–550, 2020.

[20] M. J. Kim, W. Lee, J. Y. Choi, G. Chung, K.-L. Han, I. S. Choi, C. Ott, and W. K. Chung, "A passivity-based nonlinear admittance control with application to powered upper-limb control under unknown environmental interactions," *IEEE/ASME Transactions on Mechatronics*, vol. 24, no. 4, pp. 1473–1484, 2019.

[21] A. Toedtheide, X. Chen, H. Sadeghian, A. Naceri, and S. Haddadin, "A force-sensitive exoskeleton for teleoperation: An application in elderly care robotics," in *2023 IEEE International Conference on Robotics and Automation (ICRA)*. IEEE, 2023, pp. 12 624–12 630.

[22] J. J. Craig, *Introduction to robotics, mechanics and control*. Pearson, 2014.

[23] M. Hamad, A. Kurdas, N. Mansfeld, S. Abdolshah, and S. Haddadin, "Modularize-and-conquer: A generalized impact dynamics and safe precollision control framework for floating-base tree-like robots," *IEEE Transactions on Robotics*, 2023.

[24] H. Sadeghian, L. Villani, M. Keshmiri, and B. Siciliano, "Task-space control of robot manipulators with null-space compliance," *IEEE Transactions on Robotics*, vol. 30, no. 2, pp. 493–506, 2013.

[25] Q. Wu, X. Wang, B. Chen, and H. Wu, "Development of an rbfn-based neural-fuzzy adaptive control strategy for an upper limb rehabilitation exoskeleton," *Mechatronics*, vol. 53, pp. 85–94, 2018.

[26] M. Indri, "Control of manipulators subject to unknown friction," in *Proceedings of the 45th IEEE Conference on Decision and Control*. IEEE, 2006, pp. 2943–2948.